

Evolution of Dust Temperature of Galaxies through Cosmic Time as seen by *Herschel* ^{*}

H.S. Hwang,^{1†} D. Elbaz,¹ G. Magdis,¹ E. Daddi,¹ M. Symeonidis,² B. Altieri,³ A. Amblard,⁴ P. Andreani,^{5,6} V. Arumugam,⁷ R. Auld,⁸ H. Aussel,¹ T. Babbedge,⁹ S. Berta,¹⁰ A. Blain,¹¹ J. Bock,^{11,12} A. Bongiovanni,^{13,14} A. Boselli,¹⁵ V. Buat,¹⁵ D. Burgarella,¹⁵ N. Castro-Rodríguez,^{13,14} A. Cava,^{13,14} J. Cepa,^{13,14} P. Chaniel,⁹ E. Chapin,¹⁶ R.-R. Chary,¹⁷ A. Cimatti,¹⁸ D.L. Clements,⁹ A. Conley,¹⁹ L. Conversi,³ A. Cooray,^{4,11} H. Dannerbauer,¹ M. Dickinson,²⁰ H. Dominguez,²¹ C.D. Dowell,^{11,12} J.S. Dunlop,⁷ E. Dwek,²² S. Eales,⁸ D. Farrah,²³ N. Förster Schreiber,¹⁰ M. Fox,⁹ A. Franceschini,²⁴ W. Gear,⁸ R. Genzel,¹⁰ J. Glenn,¹⁹ M. Griffin,⁸ C. Gruppioni,²⁵ M. Halpern,¹⁶ E. Hatziminaoglou,⁵ E. Ibar,²⁶ K. Isaak,⁸ R.J. Ivison,^{26,7} W.-S. Jeong,²⁷ G. Lagache,²⁸ D. Le Borgne,²⁹ E. Le Floch,¹ H.M. Lee,³⁰ J.C. Lee,³⁰ M.G. Lee,³⁰ L. Levenson,^{11,12} N. Lu,^{11,31} D. Lutz,¹⁰ S. Madden,¹ B. Maffei,³² B. Magnelli,¹⁰ G. Mainetti,²⁴ R. Maiolino,²¹ L. Marchetti,²⁴ A.M.J. Mortier,⁹ H.T. Nguyen,^{12,11} R. Nordon,¹⁰ B. O'Halloran,⁹ K. Okumura,¹ S.J. Oliver,²³ A. Omont,²⁹ M.J. Page,² P. Panuzzo,¹ A. Papageorgiou,⁸ C.P. Pearson,^{33,34} I. Pérez-Fournon,^{13,14} A.M. Pérez García,^{13,14} A. Poglitsch,¹⁰ M. Pohlen,⁸ P. Popesso,¹⁰ F. Pozzi,²⁵ J.I. Rawlings,² D. Rigopoulou,^{33,35} L. Riguccini,¹ D. Rizzo,⁹ G. Rodighiero,²⁴ I.G. Roseboom,²³ M. Rowan-Robinson,⁹ A. Saintonge,¹⁰ M. Sánchez Portal,³ P. Santini,²¹ M. Sauvage,¹ B. Schulz,^{11,31} Douglas Scott,¹⁶ N. Seymour,² L. Shao,¹⁰ D.L. Shupe,^{11,31} A.J. Smith,²³ J.A. Stevens,³⁶ E. Sturm,¹⁰ L. Tacconi,¹⁰ M. Trichas,⁹ K.E. Tugwell,² M. Vaccari,²⁴ I. Valtchanov,³ J.D. Vieira,¹¹ L. Vigroux,²⁹ L. Wang,²³ R. Ward,²³ G. Wright,²⁶ C.K. Xu^{11,31} and M. Zemcov^{11,12}

¹ Laboratoire AIM-Paris-Saclay, CEA/DSM/Irfu - CNRS - Université Paris Diderot, CE-Saclay, pt courrier 131, F-91191 Gif-sur-Yvette, France

² Mullard Space Science Laboratory, University College London, Holmbury St. Mary, Dorking, Surrey RH5 6NT, UK

³ Herschel Science Centre, European Space Astronomy Centre, Villanueva de la Cañada, 28691 Madrid, Spain

⁴ Dept. of Physics & Astronomy, University of California, Irvine, CA 92697, USA

⁵ ESO, Karl-Schwarzschild-Str. 2, 85748 Garching bei München, Germany

⁶ INAF - Osservatorio Astronomico di Trieste, via Tiepolo 11, 34143 Trieste, Italy

⁷ Institute for Astronomy, University of Edinburgh, Royal Observatory, Blackford Hill, Edinburgh EH9 3HJ, UK

⁸ Cardiff School of Physics and Astronomy, Cardiff University, Queens Buildings, The Parade, Cardiff CF24 3AA, UK

⁹ Astrophysics Group, Imperial College London, Blackett Laboratory, Prince Consort Road, London SW7 2AZ, UK

¹⁰ Max-Planck-Institut für Extraterrestrische Physik (MPE), Postfach 1312, 85741, Garching, Germany

¹¹ California Institute of Technology, 1200 E. California Blvd., Pasadena, CA 91125, USA

¹² Jet Propulsion Laboratory, 4800 Oak Grove Drive, Pasadena, CA 91109, USA

¹³ Instituto de Astrofísica de Canarias (IAC), E-38200 La Laguna, Tenerife, Spain

¹⁴ Departamento de Astrofísica, Universidad de La Laguna (ULL), E-38205 La Laguna, Tenerife, Spain

¹⁵ Laboratoire d'Astrophysique de Marseille, OAMP, Université Aix-marseille, CNRS, 38 rue Frédéric Joliot-Curie, 13388 Marseille cedex 13, France

¹⁶ Department of Physics & Astronomy, University of British Columbia, 6224 Agricultural Road, Vancouver, BC V6T 1Z1, Canada

¹⁷ Spitzer Science Center, California Institute of Technology, Pasadena, CA 91125, USA

¹⁸ Dipartimento di Astronomia, Università di Bologna, Via Ranzani 1, 40127 Bologna, Italy

¹⁹ Dept. of Astrophysical and Planetary Sciences, CASA 389-UCB, University of Colorado, Boulder, CO 80309, USA

²⁰ National Optical Astronomy Observatory, 950 North Cherry Avenue, Tucson, AZ 85719, USA

²¹ INAF-Osservatorio Astronomico di Bologna, via Ranzani 1, I-40127 Bologna, Italy

²² Observational Cosmology Lab, Code 665, NASA Goddard Space Flight Center, Greenbelt, MD 20771, USA

ABSTRACT

We study the dust properties of galaxies in the redshift range $0.1 \lesssim z \lesssim 2.8$ observed by the *Herschel Space Observatory* in the field of the Great Observatories Origins Deep Survey-North as part of PEP and HerMES key programmes. Infrared (IR) luminosity (L_{IR}) and dust temperature (T_{dust}) of galaxies are derived from the spectral energy distribution (SED) fit of the far-infrared (FIR) flux densities obtained with PACS and SPIRE instruments onboard *Herschel*. As a reference sample, we also obtain IR luminosities and dust temperatures of local galaxies at $z < 0.1$ using *AKARI* and *IRAS* data in the field of the Sloan Digital Sky Survey. We compare the $L_{\text{IR}} - T_{\text{dust}}$ relation between the two samples and find that: the median T_{dust} of *Herschel*-selected galaxies at $z \gtrsim 0.5$ with $L_{\text{IR}} \gtrsim 5 \times 10^{10} L_{\odot}$, appears to be 2–5 K colder than that of *AKARI*-selected local galaxies with similar luminosities; and the dispersion in T_{dust} for high- z galaxies increases with L_{IR} due to the existence of cold galaxies that are not seen among local galaxies. We show that this large dispersion of the $L_{\text{IR}} - T_{\text{dust}}$ relation can bridge the gap between local star-forming galaxies and high- z submillimeter galaxies (SMGs). We also find that three SMGs with very low T_{dust} ($\lesssim 20$ K) covered in this study have close neighbouring sources with similar 24- μm brightness, which could lead to an overestimation of FIR/(sub)millimeter fluxes of the SMGs.

Key words: galaxies: evolution – galaxies: formation – galaxies: general – galaxies: high-redshift – galaxies: starburst – infrared: galaxies

1 INTRODUCTION

Understanding star formation (SF) mechanisms in galaxies and how star formation rate (SFR) of galaxies evolves through cosmic time are key issues in the study of galaxy formation and evolution. The SFR is closely related to dust properties such as temperature (T_{dust}), mass, opacity, emissivity, and spatial extent. In order to investigate dust properties of galaxies, it is important to obtain data covering the complete infrared (IR) wavelength range that includes both the “Wien” and “Rayleigh-Jeans” sides of the peak of the IR spectral energy distribution (SED). Thanks to the advent of the *Herschel Space Observatory* (Pilbratt et al. 2010) with its very wide wavelength coverage (70–500 μm), we are now able to study complete IR SEDs of high- z galaxies at $z \sim 1 - 3$.

The “Rayleigh-Jeans” side of the IR SED of a galaxy is crucial for the study of dust properties, but up to now available photometric data for high- z galaxies have been limited to a small number of wavelength windows and to small regions in the sky. Despite the modest wavelength coverage of IR SEDs for high- z galaxies, it was suggested that luminous infrared galaxies (LIRGs; $10^{11} L_{\odot} < L_{\text{IR}} < 10^{12} L_{\odot}$) and ultraluminous infrared galaxies (ULIRGs; $10^{12} L_{\odot} < L_{\text{IR}} < 10^{13} L_{\odot}$) at high redshifts may be colder than their local counterparts (e.g., Rowan-Robinson et al. 2004, 2005; Sajina et al. 2006; Symeonidis et al. 2009; Seymour et al. 2010; see also Muzzin et al. 2010). For example, Symeonidis et al. (2009) found that the IR SEDs of high- z galaxies, on average, are peaked at longer wavelengths than those of local galaxies by comparing *Spitzer* 70- μm -selected galaxies at $0.1 \leq z < 2$ with *IRAS* 60- μm -selected galaxies at $z < 0.1$. They also found that the peak of IR

SEDs for local galaxies is shifted to the shorter wavelengths as IR luminosity (L_{IR}) increases, while the peak of IR SEDs for high- z galaxies is located at a wider wavelength range compared to local galaxies and varies little with L_{IR} . However, Magnelli et al. (2009), using the *Spitzer* data in the fields of Great Observatories Origins Deep Survey (GOODS; Dickinson et al. 2003) and Far Infrared Deep Extragalactic Legacy survey (FIDEL), suggested that IR SEDs of high- z galaxies at $0.4 < z < 1.3$ are not significantly different from those of local galaxies. Several studies have also been carried out which suggest that the apparent change with redshift is mainly a selection effect (e.g., Pope et al. 2006; Chapin et al. 2010).

It certainly seems that at high redshifts there are much colder populations of galaxies than local galaxies with similar IR luminosities [e.g., (sub)millimeter galaxies (SMGs), Blain et al. 2002; Chapman et al. 2005; Pope et al. 2006; Kovács et al. 2006; Huynh et al. 2007; Coppin et al. 2008; Clements et al. 2008]. The relation between IR luminosity and dust temperature has been used as a useful tool in order to understand the connection between galaxy populations such as (U)LIRGs and SMGs (Dunne et al. 2000; Chapman et al. 2003, 2005; Kovács et al. 2006; Chaniai et al. 2007; Yang et al. 2007; Younger et al. 2009; Dye et al. 2009; Chapin et al. 2009, 2010; Clements et al. 2010; Magdis et al. 2010a). Interestingly, in the $L_{\text{IR}} - T_{\text{dust}}$ plane, SMGs form a separate locus from the (U)LIRGs, which can suggest a different origin between the two.

In this paper, we investigate the IR SEDs and the dust properties of high- z galaxies by taking advantage of the wide wavelength coverage (70–500 μm) of the Photodetector Array Camera (PACS; Poglitsch et al. 2010) and Spectral and Photometric Imaging Receiver (SPIRE; Griffin et al. 2010) instruments onboard *Herschel*. In order to study how dust properties of high- z galaxies are different from those of their local counterparts, we construct a sample of galax-

* Herschel is an ESA space observatory with science instruments provided by European-led Principal Investigator consortia and with important participation from NASA.

† E-mail: hoseong.hwang@cea.fr

ies at $z < 0.1$ that were observed by the *AKARI* telescope (Murakami et al. 2007). The *AKARI* all-sky survey data contain flux density measurements up to $160\ \mu\text{m}$, which can probe the long-wavelength side of the peak of IR SEDs of local galaxies in a way similar to that of *Herschel* for high- z galaxies. Throughout, we adopt $h = 0.7$ and a flat ΛCDM cosmology with density parameters $\Omega_\Lambda = 0.73$ and $\Omega_m = 0.27$.

2 OBSERVATIONS AND DATA

GOODS-North (hereafter GOODS-N) was observed by *Herschel* as part of the Guaranteed Time Key Programmes PACS Extragalactic Probe (PEP¹) and *Herschel* Multi-tiered Extragalactic Survey (HerMES²; Oliver et al. 2010, in prep.). Source extraction on these PACS and SPIRE images was performed at the prior positions of *Spitzer* 24- μm -selected sources, and details are described in Berta et al. (2010), Magnelli et al. (2010) and Roseboom et al. (2010). PACS measurements are above the confusion limit, and we used flux densities in PACS bands down to 3σ limits of 3 and 5.7 mJy at 100 and $160\ \mu\text{m}$, respectively (Berta et al. 2010). SPIRE measurements are used down to 5σ limits of 4.4, 4.8 and 7.6 mJy at 250, 350 and $500\ \mu\text{m}$, respectively. It is noted that these measurements lie below the $1\text{-}\sigma$ SPIRE confusion limit of 5.8, 6.3, 6.8 mJy (Nguyen et al. 2010). However, this limit is a spatially averaged statistical limit which considers that galaxies are homogeneously distributed in the field and all affected in the same way by close neighbours. In this study, we flag galaxies more “isolated” than others for which SPIRE flux densities can potentially be more robust by using the higher spatial resolution 24 μm images (to be explained in §3).

By combining these catalogues with the existing multi-wavelength data, we made a band-merged catalogue of IR sources having flux density measurements at *Spitzer* MIPS 24 and $70\ \mu\text{m}$, *Herschel* PACS 100 and $160\ \mu\text{m}$, and *Herschel* SPIRE 250, 350 and $500\ \mu\text{m}$ (see Elbaz et al. 2010 for details). For 493 galaxies detected in at least one out of the five PACS/SPIRE bands, we computed the IR luminosity using the SED models of Chary & Elbaz (2001, CE01) by allowing renormalization of the templates. The SED fit was applied to the flux densities at $\lambda_{\text{rest}} \geq 30\ \mu\text{m}$, and L_{IR} for all 493 galaxies was calculated.

In order to determine the dust temperatures, we fit the observational data with a modified black body (MBB) model by fixing the emissivity parameter to $\beta = 1.5$ (Hildebrand 1983; Gordon et al. 2010). We used only the galaxies that satisfy the following conditions:

- (i) there should be at least one flux measurement shortwards to the FIR peak (i.e. $0.55\lambda_p \leq \lambda_{\text{rest}} < \lambda_p$ where λ_p is the rest-frame, peak wavelength of the best-fit CE01 SED model and λ_{rest} is the rest-frame wavelength of the observed data);
- (ii) there should be at least one flux measurement longwards to the FIR peak (i.e. $\lambda_p \leq \lambda_{\text{rest}}$); and

- (iii) the FIR SED should be physical (convex, not concave), i.e. we reject galaxies with $(S_{100} \text{ or } S_{160}) \geq S_{250}$ and $S_{250} \leq (S_{350} \text{ or } S_{500})$, or $(S_{100} \text{ or } S_{160}) \geq S_{350}$ and $S_{350} \leq S_{500}$.

The above criteria ensure a well-sampled SED around the peak of the FIR emission, and the wavelength cut of $0.55\lambda_p$ is introduced to reduce the contribution of warm dust (i.e. emission from very small grains). For these galaxies, we fit the flux densities at $\lambda_{\text{rest}} \geq 0.55\lambda_p$ using the MBB model. We then select galaxies having flux measurements on both sides of the peak for the best-fit MBB model, and secure a final sample of 140 galaxies. Uncertainties of L_{IR} and T_{dust} were computed by randomly selecting flux densities at each band within the associated error distribution (assumed to be Gaussian) and then re-fitting. It is noted that we checked how T_{dust} measurements of galaxies are affected if we remove some data points for the fit. We found that T_{dust} becomes systematically lower/higher if you use only data points shortwards/longwards to the FIR peak. However, T_{dust} does not change systematically even if you remove some data points at $\lambda_{\text{rest}} \geq 0.55\lambda_p$ for the fit as long as you have measurements on both sides of the peak wavelength.

For local galaxies, we construct an IR catalogue by cross-correlating our IR sources with the galaxies in the redshift catalogue as follows. We use the *IRAS* Faint Sources Catalog – Version 2 (Moshir et al. 1992), which contains 173,044 sources with flux density measurements at 12, 25, 60 and $100\ \mu\text{m}$. We also use the *AKARI*/Far-Infrared Surveyor (FIS; Kawada et al. 2007) all-sky survey Bright Source Catalogue (BSC³) ver. 1.0 that contains 427,071 sources over the whole sky, with measured flux densities at 65, 90, 140 and $160\ \mu\text{m}$. Among the measurements at *IRAS* and *AKARI* bands, we consider only the reliable⁴ flux densities. For the redshift catalogue, we use a spectroscopic sample of galaxies in the Sloan Digital Sky Survey Data Release 7 (Abazajian et al. 2009, SDSS DR7) complemented by a photometric sample of galaxies whose redshift information is available in the literature (Hwang et al. 2010).

By adopting the same method applied to high- z galaxies, we compute L_{IR} for the local galaxies by fitting the CE01 templates to the flux densities at $\lambda_{\text{rest}} \geq 30\ \mu\text{m}$. For T_{dust} estimates, in addition to the conditions (i) and (ii) used for high- z galaxies, we use only sources detected at 140 or $160\ \mu\text{m}$. This condition ensures a fair comparison with the high- z samples as in both samples have flux density measurements longwards to the FIR peak. Since *IRAS* 60 μm and *AKARI* 65 μm (or *IRAS* 100 μm and *AKARI* 90 μm) partially overlap, we use only *IRAS* data (S_{60} and S_{100}) for the fit to avoid over-weighting when both *IRAS* and *AKARI* flux densities are measured. Finally, we use only the galaxies having flux density measurements on both sides of the peak of the best-fit MBB model.

Fig. 1 represents example SEDs for a high- z galaxy in GOODS-N and a local galaxy in SDSS with the best-fits CE01 and MBB models. In Fig. 2, we plot L_{IR} and T_{dust} for

³ http://www.ir.isas.jaxa.jp/AKARI/Observation/PSC/Public/RN/AKARI-FIS_BSC_V1_RN.pdf

⁴ Flux quality flags are either ‘high’ or ‘moderate’ for *IRAS* sources and ‘high’ for *AKARI* sources.

¹ <http://www.mpe.mpg.de/ir/Research/PEP>

² <http://hermes.sussex.ac.uk>

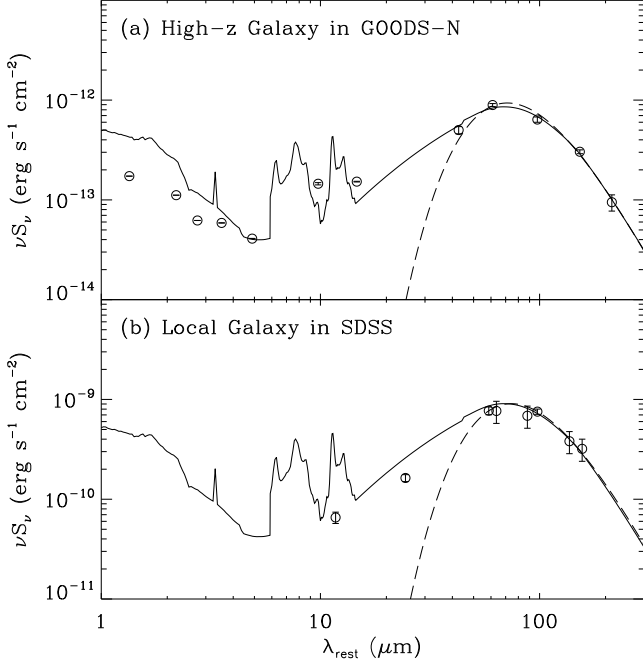


Figure 1. Example SEDs for (a) a high- z galaxy in GOODS-N with $L_{\text{IR}} = 6.7 \times 10^{11} (L_{\odot})$, $T_{\text{dust}} = 37$ K, and $z = 0.64$; (b) a local galaxy in SDSS with $L_{\text{IR}} = 4.9 \times 10^{11} (L_{\odot})$, $T_{\text{dust}} = 35$ K, and $z = 0.02$. The best-fit CE01 and MBB models are indicated by solid and dashed lines, respectively.

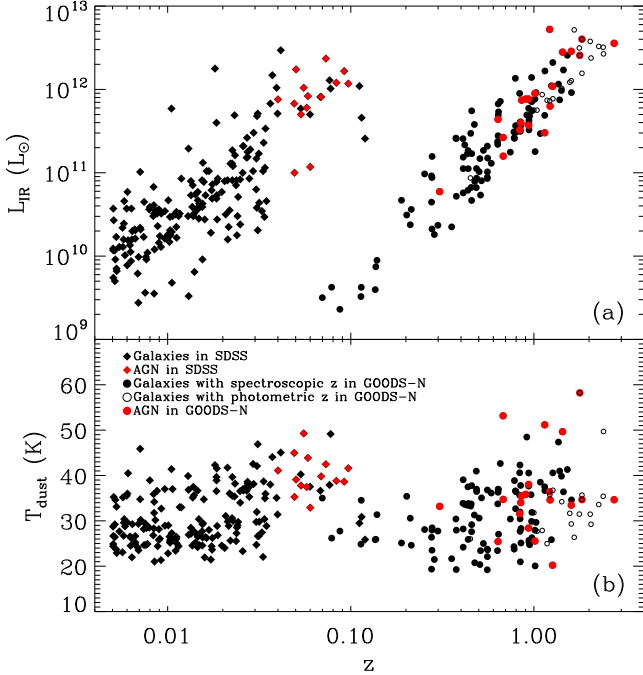


Figure 2. (a) L_{IR} and (b) T_{dust} for 140 galaxies in GOODS-N (circles) and 190 galaxies in SDSS (diamonds) vs. redshift. Galaxies with spectroscopic and photometric redshifts are filled and open circles, respectively. Galaxies hosting AGN are indicated by red symbols.

140 high- z and 190 local galaxies as a function of redshift, which shows that the two samples are distributed over similar ranges of L_{IR} and T_{dust} . The high- z galaxies in GOODS-N are found at $0.07 < z < 2.74$ with $2.3 \times 10^9 (L_{\odot}) < L_{\text{IR}} < 5.3 \times 10^{12} (L_{\odot})$ and $19 (K) < T_{\text{dust}} < 58 (K)$, while the local galaxies in SDSS are in the range $0.005 < z < 0.119$ with $2.7 \times 10^9 (L_{\odot}) < L_{\text{IR}} < 3.0 \times 10^{12} (L_{\odot})$ and $21 (K) < T_{\text{dust}} < 49 (K)$.

3 RESULTS

We show the relation between L_{IR} and T_{dust} for local and high- z samples in Figs. 3 and 4, respectively. Fig. 3 shows the distribution of local galaxies in comparison with known ULIRGs and SMGs in the literature. We determine a smoothed median trend of T_{dust} as a function of L_{IR} for our local galaxies. Since the contribution of active galactic nuclei (AGN) to determining the median trend of T_{dust} for local and high- z galaxies could be different, we exclude them when determining the median. We call AGN those sources whose optical spectral types are found to be Seyferts, low-ionization nuclear emission-line regions (LINERs) or composite galaxies in the emission line ratio diagram (Baldwin et al. 1981; Kewley et al. 2006). We classify only the galaxies at $z > 0.04$ as AGN due to the problem of the small ($3''$) fixed-size aperture for SDSS spectroscopy (Kewley et al. 2006). It is seen that T_{dust} remains constant in the lower end of the luminosity range ($L_{\text{IR}} \lesssim 5 \times 10^{10} L_{\odot}$) and increases as L_{IR} increases. This trend has been indicated in the previous studies by a shift of the peak in the IR SED with increasing L_{IR} (Soifer et al. 1987, 1989; Chapman et al. 2003; Chapin et al. 2009; Symeonidis et al. 2009; see also Amblard et al. 2010). At $L_{\text{IR}} \gtrsim 10^{12} (L_{\odot})$, our samples are smoothly connected to the locus of known ULIRGs at intermediate/high redshifts. We also note that changing AGN selection criteria has a small effect on our results.

In Fig. 4(a), we plot high- z galaxies along with the loci of ULIRGs, SMGs and local SDSS galaxies. The median trend of T_{dust} for high- z galaxies is also determined by excluding those galaxies hosting X-ray selected AGN as well as possibly blended sources. AGN have either $L_{\text{X}}[0.5-8.0 \text{ keV}] > 3 \times 10^{42} \text{ ergs s}^{-1}$, a hardness ratio (ratio of the counts in the 2–8 keV to 0.5–2 keV passbands) greater than 0.8, $N_{\text{H}} \geq 10^{22} \text{ cm}^{-2}$, or broad/high-ionization AGN emission lines (Bauer et al. 2004). We regard a galaxy as ‘blended’ if it has at least one neighbouring source within \sim one beam FWHM of the galaxy position at $24 \mu\text{m}$ and SPIRE images ($20''$ for $24 \mu\text{m}$ and $250 \mu\text{m}$, $27''$ for $350 \mu\text{m}$, and $46''$ for $500 \mu\text{m}$). For the $24\text{-}\mu\text{m}$ image, the criterion is at least two neighbouring sources instead of one. In addition, we require that the flux density of a neighbouring source should be larger than 50% of that of the galaxy. Among 140 high- z galaxies, we have 84 ‘clean’ and 56 ‘blended’ galaxies (see also Brisbin et al. 2010 for a purity index that is a measure of blending of a galaxy). Fig. 4(b) represents the distribution of T_{dust} for ‘clean’ and ‘blended’ galaxies including AGN. This shows that only ‘blended’ galaxies have several cold galaxies with $T_{\text{dust}} \sim 20$ K, while ‘clean’ galaxies do not (to be discussed in detail in §4.2).

In Fig. 4(a), the median trend of T_{dust} for high- z galax-

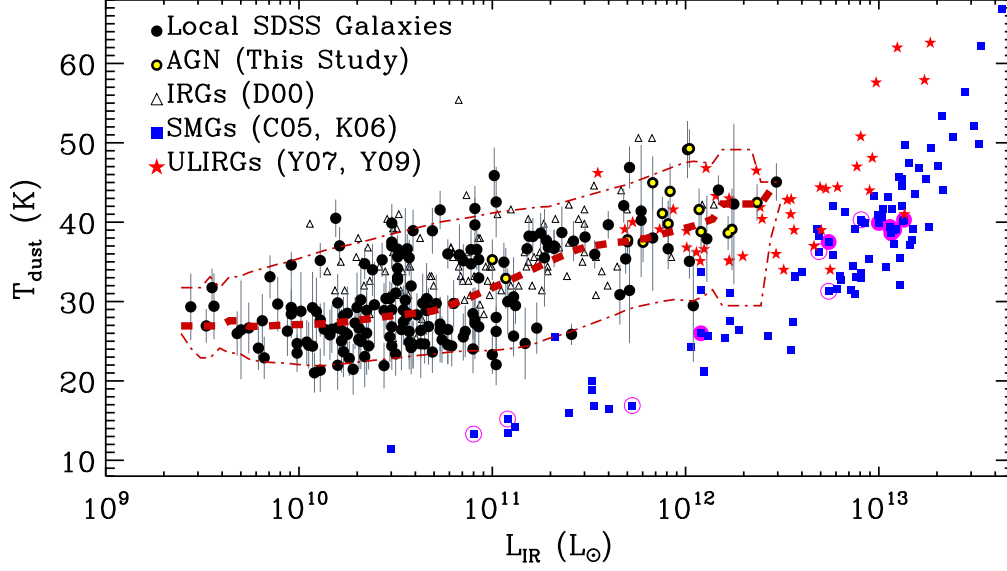


Figure 3. T_{dust} vs. L_{IR} for galaxies in SDSS. Galaxies hosting AGN are indicated by yellow symbols. The thick dashed line is a smoothed median trend of T_{dust} for local SDSS galaxies by excluding those with AGN, and the dot-dashed lines are its envelope that includes 90% of the galaxies above and below the median. The known local infrared galaxies (IRGs) (D00: Dunne et al. 2000), SMGs (C05: Chapman et al. 2005, K06: Kovács et al. 2006) and ULIRGs (Y07: Yang et al. 2007, Y09: Younger et al. 2009) are plotted with triangles, squares and star symbols, respectively. Among the SMGs in common between this study and C05, those having no neighbouring sources (clean) are denoted by large filled circles, while those possibly contaminated by neighbouring sources (blended) are denoted by large open circles.

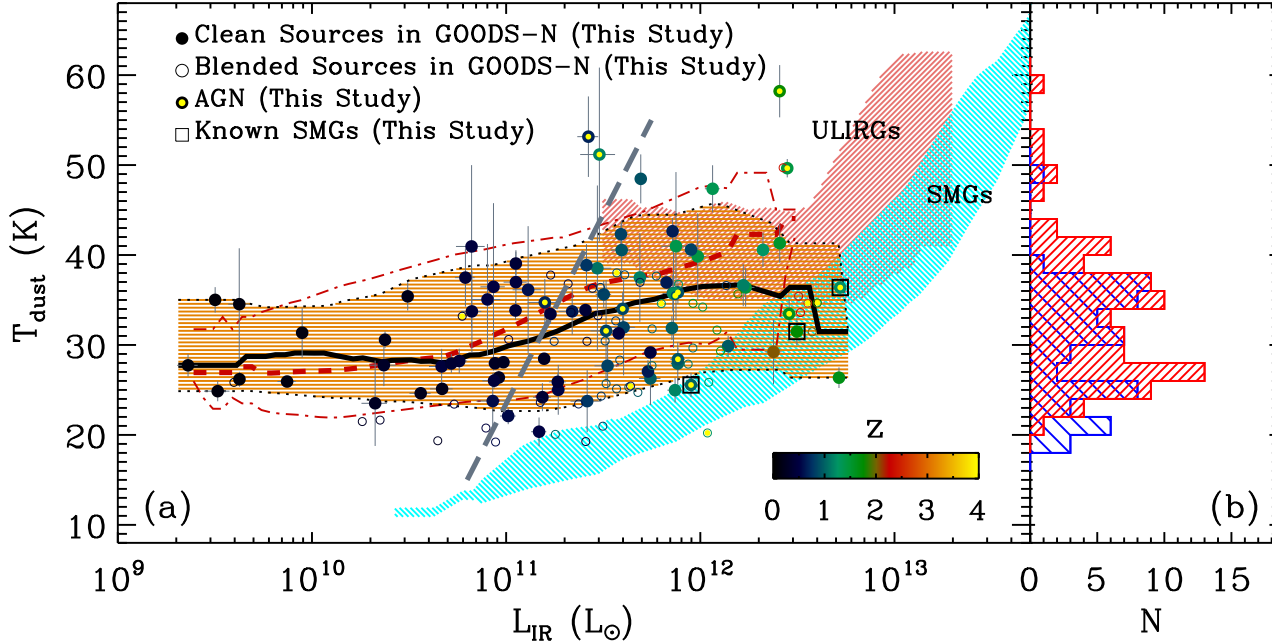


Figure 4. (a) T_{dust} vs. L_{IR} for galaxies in GOODS-N. Galaxies hosting AGN are indicated by yellow symbols. The thick dashed line is a smoothed median trend of T_{dust} for local galaxies adopted in Fig. 3, and the dot-dashed lines are its 90% envelope. The loci of known SMGs and ULIRGs in Fig. 3 are plotted as regions filled by cyan and coral colour, respectively. Clean and blended galaxies are denoted by filled and open circles, respectively. The thick solid line is a median trend of T_{dust} for galaxies in the GOODS-N field and the dotted lines are its 90% envelope (filled with orange colour). Inclined, grey long-dashed lines indicate the *AKARI* selection function at the maximum redshift of local galaxies ($z = 0.119$). (b) Distribution of T_{dust} for high- z galaxies. Clean and blended galaxies including AGN are denoted by hatched histograms with orientation of 45° (// with red colour) and of 315° (\ \ with blue colour) relative to horizontal, respectively.

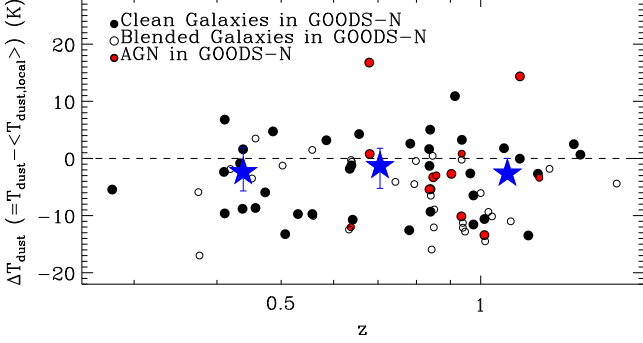


Figure 5. Deviation of T_{dust} (ΔT_{dust}) for high- z LIRGs from the median trend of local LIRGs vs. redshift. Filled and open symbols are ‘clean’ and ‘blended’ galaxies, respectively. Star symbol represents the median value of ΔT_{dust} for ‘clean’ galaxies in each redshift bin.

ies also appears fairly constant at low luminosities, but increases as L_{IR} increases at higher luminosities. By comparing with local galaxies, we see that the median trend of T_{dust} for *Herschel*-selected high- z galaxies at $z \gtrsim 0.5$ becomes smaller than that for *AKARI*-selected low- z galaxies by 2 – 5 K at high luminosities ($L_{\text{IR}} > 5 \times 10^{10} L_{\odot}$). Note that this does not necessarily mean that high- z galaxies are systematically colder than local galaxies with similar luminosities (to be discussed in §4.1). It is also seen that T_{dust} scatter increases by about 5 K in the sense that the upper envelope for high- z galaxies is similar to that of local galaxies, while the lower envelope for high- z galaxies stretches below. These results are consistent with the results based on the peak position of the IR SEDs (Symeonidis et al. 2009). Interestingly, the high- z galaxies with low T_{dust} fill the gap between local star-forming galaxies and high- z SMGs in the $L_{\text{IR}} - T_{\text{dust}}$ plane. It is also interesting that T_{dust} for AGN follows a similar trend as for star-forming galaxies, which indicates that the star formation of galaxies having AGN does not significantly differ from that of normal star-forming galaxies seen in the FIR regime, where SF dominates the IR emission of AGN (Elbaz et al. 2010; Shao et al. 2010; Hatziminaoglou et al. 2010).

To investigate how T_{dust} for high- z galaxies evolves with redshift compared to local galaxies with similar L_{IR} , in Fig. 5, we plot the deviation of T_{dust} for high- z LIRGs from the median trend ($\langle T_{\text{dust,local}} \rangle$, thick dashed line in Fig. 4a) of T_{dust} for local LIRGs ($\Delta T_{\text{dust}} = T_{\text{dust}} - \langle T_{\text{dust,local}} \rangle$) as a function of redshift. This shows that ΔT_{dust} is negative, on average, which indicates that *Herschel*-selected high- z LIRGs at $0.3 < z < 1.4$ appear to be colder than *AKARI*-selected local LIRGs. ΔT_{dust} changes little with redshift, but it is difficult to draw any strong conclusions due the small sample size. Since the deeper observation of GOODS fields will be conducted in PEP and in the GOODS-*Herschel* key programme (PI: D. Elbaz), the future *Herschel* data will help us to address this issue with a larger number of galaxies up to higher redshift.

To investigate how the SEDs of high- z galaxies are different from the local SED templates of CE01, we plot the average SEDs (from UV to FIR) of *cold* and *normal* LIRGs at high redshifts in comparison with the local SED templates of CE01 in Fig. 6. The high- z galaxies are classified

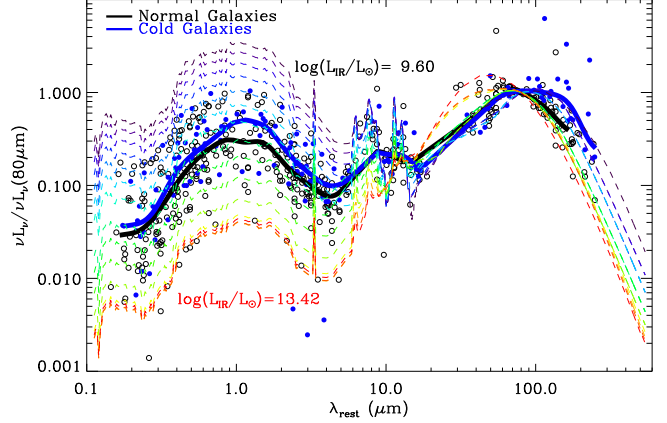


Figure 6. Average SEDs of LIRGs in GOODS-N with spectroscopic redshifts normalized by the luminosity at 80 μm . Observed data for 10 *cold* and 26 *normal* galaxies are plotted by filled and open circles, respectively. The average SEDs of the data points are plotted as solid lines. Colour-coded dashed lines are CE01 templates normalized by the luminosity at 80 μm , and L_{IR} of the templates with the maximum and the minimum L_{IR} are labelled.

into three groups by comparing their T_{dust} values with the median trend of T_{dust} for local galaxies (thick dashed line in Fig. 4a): *cold* (those with T_{dust} values less than the lower envelope of local galaxies); *normal* (those with T_{dust} values within the envelopes of local galaxies); and *warm* (those with T_{dust} values larger than the upper envelope of local galaxies). Fig. 6 shows that the peak wavelength of the FIR SED for *cold* galaxies is larger than that for *normal* galaxies as expected. The average FIR SED of *normal* galaxies appears to match well with the CE01 template of similar luminosity, but that of *cold* galaxies is matched with roughly 80 times less luminous template, even if the median L_{IR} of *normal* and *cold* galaxies are similar ($\langle L_{\text{IR}}/L_{\odot} \rangle \sim 5 \times 10^{11}$ and $4 \times 10^{11} L_{\odot}$ for *normal* and *cold* galaxies, respectively).

We wish to emphasize that the longer-wavelength side of the peak of the FIR SED for *cold* galaxies could be affected by blending at long wavelengths. Since the beam FWHM gets larger as wavelength increases, the flux densities at longer wavelength can be systematically overestimated if there is more than one source within the resolution limit. In addition, galaxies having neighbouring sources seem to have low T_{dust} compared to ‘clean’ galaxies, as seen in Fig. 4(b), which suggests that we should be cautious when we measure T_{dust} using multi-wavelength data with different resolutions. We have calculated the fraction of blended galaxies among *normal* and *cold* galaxies, and find values of $34 \pm 6\%$ and $58 \pm 9\%$, respectively. We have tried to eliminate such problem in our samples by identifying blended galaxies, and by using the FIR source catalogue based on prior extraction (Berta et al. 2010; Roseboom et al. 2010). However, since we may not have completely deblend all sources and do not account for galaxies whose neighbours are less bright than 50% of the target galaxy, there could be a remaining contribution to the FIR flux of *cold* galaxies due to this effect.

Interestingly, the *cold* galaxies are brighter than the *normal* galaxies in the optical bands. This could imply that there is a correlation between T_{dust} and the optical proper-

ties such as galaxy morphology, colour, or size. Thus, the study of the relation between optical properties and T_{dust} may provide us useful hints for the origin of the *cold* galaxies (Le Floc'h et al. 2010, in prep.).

4 DISCUSSION

4.1 Selection Effects

The *AKARI* data contain flux density measurements up to $\lambda = 160 \mu\text{m}$ ($\lambda_{\text{rest}} = 157 \mu\text{m}$ with a median redshift of $z = 0.015$ for local samples), while *Herschel* data have measurements up to $\lambda = 500 \mu\text{m}$ ($\lambda_{\text{rest}} = 330 \mu\text{m}$ with a median redshift of $z = 0.5$ for high- z samples). Therefore, the T_{dust} difference between the two samples seen in Fig. 4(a) could be affected by the difference in selection effects. For example, Chapin et al. (2010) found results similar to this study, in the sense that the dust temperatures of *BLAST*-selected ($250\text{--}500 \mu\text{m}$) high- z galaxies at $z < 3$ are systematically cooler than *IRAS* $60\text{-}\mu\text{m}$ -selected local galaxies. When they account the difference in selection effects between the two samples, they find no evidence for evolution of T_{dust} . On the other hand, if we consider *Herschel*-selected local galaxies ($z < 0.1$) observed in the *Herschel*-ATLAS key programme (Eales et al. 2010), we can find cold galaxies with $T_{\text{dust}} \lesssim 20 \text{ K}$ that are not seen in our local sample (see Fig. 2 in Amblard et al. 2010). This seems to support the idea that the different selection effects between local and high- z galaxies can explain the T_{dust} difference. However, note that there are few local galaxies with $L_{\text{IR}} \sim 10^{11} - 10^{12} L_{\odot}$ ($z < 0.1$) in the sample of Amblard et al. (2010, see their Fig. 3), which are crucial for understanding the T_{dust} difference between local and high- z galaxies (see Fig. 4a). Since a wider area will eventually be covered by the *Herschel*-ATLAS program, the upcoming data will help us to address this issue.

To investigate the effect of the different selection effect (i.e. observed wavelength and detection limit) on the difference of T_{dust} between local and high- z galaxies, and on the existence of cold galaxies ($T_{\text{dust}} \lesssim 27 \text{ K}$ and $L_{\text{IR}} > 3 \times 10^{11} L_{\odot}$) that are not seen in the local sample but seen in the high- z sample, we made a following experiment: we move the best-fit SEDs of high- z galaxies to local universe, and check whether they can be observed with *AKARI* detection limit used for local galaxies in this study. If we move all 140 high- z galaxies in Fig. 4 to $z = 0.015$ that is a median redshift of local galaxies, the expected flux densities at 140 and $160 \mu\text{m}$ for more than 99% galaxies are above the minimum values of flux densities for our local samples ($S_{140} = 1.9$ and $S_{160} = 0.25 \text{ Jy}$), which means that no galaxies would be missed with the *AKARI* detection limit. This confirms that the existence of cold galaxies at high redshifts that are not seen in the local sample, is not simply because of the different selection effect.

For the extreme case, if we move high- z galaxies to $z = 0.119$ that is a maximum redshift of local galaxies, 67% of the galaxies would be observed. The effect of the *AKARI* detection limits in the $T_{\text{dust}} - L_{\text{IR}}$ plane is shown as a thick long-dashed line in Fig. 4. Galaxies lying on the right of this line would be detected. The steep slope of the line, indicates that the *AKARI* detection limit does not affect T_{dust} distribution significantly. Moreover, cold galaxies with $T_{\text{dust}} \lesssim 27$

K and $L_{\text{IR}} > 3 \times 10^{11} L_{\odot}$ are free from this selection effect. This again confirms that the existence of cold galaxies at high redshifts is not because of the difference in selection effects.

To check how T_{dust} measurements for our local galaxies become different if we had flux measurements at longer wavelengths ($\lambda > 160 \mu\text{m}$) like for high- z galaxies, we have re-estimated T_{dust} for 44 galaxies found in common between this study and Dunne et al. (2000, D00) by combining our flux densities with $850 \mu\text{m}$ observations from D00. We found that the two estimates agree very well with a median difference of 0.2 K (rms scatter of 1.8 K). In addition, when we compare the observed $850 \mu\text{m}$ flux density in D00 with the expected flux density from our best-fit MBB model without $850 \mu\text{m}$ data, two flux densities agree well within the errors. These also indicate that T_{dust} estimates with *AKARI* bands are not biased toward high T_{dust} .

4.2 Cold Galaxies at high redshifts

T_{dust} for galaxies is a function of total SFR per unit dust mass, the dust emissivity, and the geometry, which are closely related to the global star formation efficiency (SFE). This SFE is known to be controlled by the gas density (Schmidt 1959; Kennicutt 1998), which is connected to the spatial extent of star-forming regions. Therefore, the existence of *cold* galaxies at high redshifts may imply that the spatial distribution of dust in these galaxies is more extended than that in local galaxies with similar L_{IR} . This is consistent with CO observational results for some high- z galaxies (Tacconi et al. 2006; Iono et al. 2009; Daddi et al. 2010; Tacconi et al. 2010; Genzel et al. 2010; see also Kaviani et al. 2003). On the other hand, the existence of *cold* galaxies at high redshifts may indicate large dust masses for these galaxies compared to local galaxies. If we assume similar gas-to-dust ratios for local and high- z galaxies at a given L_{IR} , the detection of a large gas content in high- z galaxies compared to local galaxies could support our results (Tacconi et al. 2006, 2010; Daddi et al. 2010).

Interestingly, the *cold* galaxies at high redshifts ($0.3 \lesssim z \lesssim 1.4$) in Fig. 4(a), fill the gap between local star-forming galaxies and high- z SMGs, connecting the two populations (see also Magdis et al. 2010b). It is noted that previous studies on T_{dust} measurement of SMGs were based on only a few photometric data points that cover only long-wavelength side of the thermal SEDs. Therefore, it is necessary to re-estimate T_{dust} for SMGs using *Herschel* data to check how the locus of SMGs in the $L_{\text{IR}} - T_{\text{dust}}$ plane changes (Magnelli et al. 2010; Chania et al. 2010, in prep.; Chapman et al. 2010, in prep.). There are 13 SMGs in common between this study and Chapman et al. (2005). Among them, we have three SMGs with T_{dust} measured in this study (T_{dust} for the other ten galaxies are not measured because they did not fulfil the selection criteria in §2 due to the low signal-to-noise ratios in some bands), and show them as squares in Fig. 4(a). They are found to be in the locus of known SMGs, indicating that our measurements are consistent with those with ground-based submillimeter studies. However, we can not determine T_{dust} for SMGs at $3 \times 10^{10} L_{\odot} \lesssim L_{\text{IR}} \lesssim 7 \times 10^{11} L_{\odot}$, which is important for understanding the connection between local galaxies and SMGs (discussed in Magnelli et al. 2010).

For these 13 SMGs, we have checked the ‘clean’ flag defined in this study, and show them in Fig. 3: there are seven ‘clean’ and six ‘blended’ galaxies. The three SMGs with T_{dust} values measured in this study, are found to be ‘clean’ galaxies. However, other three SMGs with $T_{\text{dust}} < 20$ K in Fig. 3 are found to be ‘blended’ galaxies. We have checked whether or not the redshifts of neighbouring sources are different from these SMGs, and found that the redshifts of close neighbours for two SMGs (J123636.75 + 621156.1 and J123651.76 + 621221.3) are not similar to their companion SMGs. This indicates that the low T_{dust} of SMGs could be caused by an overestimation of the FIR/(sub)millimeter fluxes due to blending problems. One SMG (J123721.87 + 621035.3 at $z \sim 0.978$) has a close neighbour at $z \sim 0.969$ that is separated by $8.6''$ (~ 70 kpc), which suggests that galaxies in an interacting pair could be colder than isolated galaxies (e.g., Tacconi et al. 2006). This issue – the relation between the galaxy merging stage and T_{dust} – needs to be investigated with a large number of galaxies.

ACKNOWLEDGMENTS

PACS has been developed by a consortium of institutes led by MPE (Germany) and including UVIE (Austria); KU Leuven, CSL, IMEC (Belgium); CEA, LAM (France); MPIA (Germany); INAF/IFSI/OAA/OAP/OAT, LENS, SISSA (Italy); IAC (Spain). This development has been supported by the funding agencies BMVIT (Austria), ESA-PRODEX (Belgium), CEA/CNES (France), DLR (Germany), ASI/INAF (Italy), and CICYT/MCYT (Spain). SPIRE has been developed by a consortium of institutes led by Cardiff University (UK) and including Univ. Lethbridge (Canada); NAOC (China); CEA, LAM (France); IFSI, Univ. Padua (Italy); IAC (Spain); SNSB (Sweden); Imperial College London, RAL, UCL-MSSL, UKATC, Univ. Sussex (UK); and Caltech, JPL, NHSC, Univ. Colorado (USA). This development has been supported by national funding agencies: CSA (Canada); NAOC (China); CEA, CNES, CNRS (France); ASI (Italy); MCINN (Spain); Stockholm Observatory (Sweden); STFC (UK); and NASA (USA). The HerMES data was accessed through the HeDaM database (<http://hedam.oamp.fr>) operated by CeSAM and hosted by the Laboratoire d’Astrophysique de Marseille. This research is based on observations with AKARI, a JAXA project with the participation of ESA. MGL was supported by the a National Research Foundation of Korea (NRF) grant funded by the Korea Government (MEST) (grant no. R01-2007-000-20336-0).

REFERENCES

Abazajian K. N., et al., 2009, *ApJS*, 182, 543
 Amblard A., et al., 2010, *A&A*, in press (arXiv:1005.2412)
 Baldwin J. A., Phillips M. M., Terlevich R., 1981, *PASP*, 93, 5
 Bauer F. E., Alexander D. M., Brandt W. N., Schneider D. P., Treister E., Hornschemeier A. E., Garmire G. P., 2004, *AJ*, 128, 2048
 Berta S., et al., 2010, *A&A*, in press (arXiv:1005.1073)

Blain A. W., Smail I., Ivison R. J., Kneib J., Frayer D. T., 2002, *Phys. Rep.*, 369, 111
 Brisbin D., et al., 2010, *MNRAS*, submitted
 Chanial P., Flores H., Guiderdoni B., Elbaz D., Hammer F., Vigroux L., 2007, *A&A*, 462, 81
 Chapin E. L., et al., 2010, *MNRAS*, submitted (arXiv:1003.2647)
 Chapin E. L., Hughes D. H., Aretxaga I., 2009, *MNRAS*, 393, 653
 Chapman S. C., Blain A. W., Smail I., Ivison R. J., 2005, *ApJ*, 622, 772
 Chapman S. C., Helou G., Lewis G. F., Dale D. A., 2003, *ApJ*, 588, 186
 Chary R., Elbaz D., 2001, *ApJ*, 556, 562
 Clements D. L., Dunne L., Eales S., 2010, *MNRAS*, 403, 274
 Clements D. L., et al., 2008, *MNRAS*, 387, 247
 Coppin K., et al., 2008, *MNRAS*, 384, 1597
 Daddi E., et al., 2010, *ApJ*, 713, 686
 Dickinson M., Giavalisco M., GOODS Team 2003, in R. Bender & A. Renzini ed., *The Mass of Galaxies at Low and High Redshift The Great Observatories Origins Deep Survey*. pp 324–+
 Dunne L., Eales S., Edmunds M., Ivison R., Alexander P., Clements D. L., 2000, *MNRAS*, 315, 115
 Dye S., et al., 2009, *ApJ*, 703, 285
 Eales S., et al., 2010, *PASP*, in press (arXiv:0910.4279)
 Elbaz D., et al., 2010, *A&A*, in press (arXiv:1005.2859)
 Genzel R., et al., 2010, *MNRAS*, in press (arXiv:1003.5180)
 Gordon K. D., et al., 2010, *A&A*, in press (arXiv:1005.3123)
 Griffin M., et al., 2010, *A&A*, in press
 Hatziminaoglou E., et al., 2010, *A&A*, in press (arXiv:1005.2192)
 Hildebrand R. H., 1983, *QJRAS*, 24, 267
 Huynh M. T., Pope A., Frayer D. T., Scott D., 2007, *ApJ*, 659, 305
 Hwang H. S., David E., Lee J. C., Jeong W.-S., Park C., Lee M. G., Lee H. M., 2010, *A&A*, in press (arXiv:1006.2166)
 Iono D., et al., 2009, *ApJ*, 695, 1537
 Kaviani A., Haehnelt M. G., Kauffmann G., 2003, *MNRAS*, 340, 739
 Kawada M., et al., 2007, *PASJ*, 59, 389
 Kennicutt Jr. R. C., 1998, *ApJ*, 498, 541
 Kewley L. J., Groves B., Kauffmann G., Heckman T., 2006, *MNRAS*, 372, 961
 Kovács A., Chapman S. C., Dowell C. D., Blain A. W., Ivison R. J., Smail I., Phillips T. G., 2006, *ApJ*, 650, 592
 Magdis G. E., et al., 2010a, *ApJ*, in press (arXiv:1007.3846)
 Magdis G. E., et al., 2010b, *MNRAS*, in press (arXiv:1007.4900)
 Magnelli B., Elbaz D., Chary R. R., Dickinson M., Le Borgne D., Frayer D. T., Willmer C. N. A., 2009, *A&A*, 496, 57
 Magnelli B., et al., 2010, *A&A*, in press (arXiv:1005.1154)
 Moshir M., Kopman G., Conrow T. A. O., 1992, *IRAS Faint Source Survey*, Explanatory supplement version 2
 Murakami H., et al., 2007, *PASJ*, 59, 369
 Muzzin A., van Dokkum P., Kriek M., Labbe I., Cury I., Marchesini D., Franx M., 2010, *ApJ*, submitted (arXiv:1003.3479)
 Nguyen H. T., et al., 2010, *A&A*, in press (arXiv:1005.2207)

- Pilbratt G. L., et al., 2010, A&A, in press
Poglitsch A., et al., 2010, A&A, in press (arXiv:1005.1487)
Pope A., et al., 2006, MNRAS, 370, 1185
Roseboom I. G., et al., 2010, MNRAS, submitted
Rowan-Robinson M., et al., 2004, MNRAS, 351, 1290
Rowan-Robinson M., et al., 2005, AJ, 129, 1183
Sajina A., Scott D., Dennefeld M., Dole H., Lacy M., Lagache G., 2006, MNRAS, 369, 939
Schmidt M., 1959, ApJ, 129, 243
Seymour N., Symeonidis M., Page M. J., Huynh M., Dwelly T., McHardy I. M., Rieke G., 2010, MNRAS, 402, 2666
Shao L., et al., 2010, A&A, in press (arXiv:1005.2562)
Soifer B. T., Boehmer L., Neugebauer G., Sanders D. B., 1989, AJ, 98, 766
Soifer B. T., Sanders D. B., Madore B. F., Neugebauer G., Danielson G. E., Elias J. H., Lonsdale C. J., Rice W. L., 1987, ApJ, 320, 238
Symeonidis M., Page M. J., Seymour N., Dwelly T., Coppin K., McHardy I., Rieke G. H., Huynh M., 2009, MNRAS, 397, 1728
Tacconi L. J., et al., 2006, ApJ, 640, 228
Tacconi L. J., et al., 2010, Nat, 463, 781
Yang M., Greve T. R., Dowell C. D., Borys C., 2007, ApJ, 660, 1198
Younger J. D., et al., 2009, ApJ, 704, 803